

Interactions Among the Brain Default-Mode, Salience, and Central-Executive Networks During Perceptual Decision-Making of Moving Dots

Ganesh B. Chand¹ and Mukesh Dhamala¹⁻³

Abstract

Cognitively demanding goal-directed tasks in the human brain are thought to involve the dynamic interplay of several large-scale neural networks, including the default-mode network (DMN), salience network (SN), and central-executive network (CEN). Resting-state functional magnetic resonance imaging (rsfMRI) studies have consistently shown that the CEN and SN negatively regulate activity in the DMN, and this switching is argued to be controlled by the right anterior insula (rAI) of the SN. However, what remains to be investigated is the pattern of directed network interactions during difficult perceptual decision-making tasks. We recorded fMRI data while participants categorized the left–right motion of moving dots. We defined regions of interest, extracted fMRI time series, and performed directed connectivity analysis using Granger causality techniques. Our analyses demonstrated that the slow oscillation (0.07–0.19 Hz) mediated the interactions within and between the DMN, SN, and CEN nodes both for easier and harder decision-making tasks. We found that the rAI, a key node of the SN, played a causal control over the DMN and CEN for easier decision-making tasks. The combined effort of the rAI and dorsal anterior cingulate cortex of the SN had the causal control over the DMN and CEN for a harder task. These findings provide important insights into how a sensory signal organizes among the DMN, SN, and CEN during sensory information-guided, goal-directed tasks.

Key words: cognitive control; effective connectivity; functional magnetic resonance imaging; Granger causality; slow frequency fluctuations

Introduction

PREVIOUS RESEARCH HAS DESCRIBED a set of large-scale, intrinsically organized brain networks underlying a broad range of functions, from basic sensory and motor capacities to cognition and higher level functions such as selecting, switching, and attending to salience events in the surrounding (Becerra et al., 2011; Deco et al., 2011; Power et al., 2011; Seeley et al., 2007). Studies have identified the existence of at least three canonical networks: (1) the default-mode network (DMN) that includes the posterior cingulate cortex (PCC) and ventromedial prefrontal cortex (VMPFC); (2) the salience network (SN) that has the right anterior insula (rAI) and dorsal anterior cingulate cortex (DACC); and (3) the central-executive network (CEN), whose key regions include the posterior parietal cortex (PPC) and dorsolateral prefrontal cortex (DLPFC) (Chen et al., 2013; Uddin, 2015).

Resting-state functional magnetic resonance imaging (rsfMRI) studies have consistently shown that the CEN and/or SN negatively regulate activity in the DMN (Chen et al., 2013; Fox et al., 2005; Fransson, 2005). However, what remains to be understood is how the activity of these networks, identified in the rsfMRI, relates to their function in cognitively demanding goal-directed tasks such as perceptual decision-making (PDM).

There are two competing lines of evidence in trying to explain how sensory signal enters SN (Ham et al., 2013) and SN might mediate interactions between DMN and CEN. One line of evidence suggests that the DACC monitors performance and its role is important for behavioral adaptation (Ridderinkhof et al., 2004). Activity in the DACC indicates an enhanced cognitive control, and its interactions with the lateral prefrontal structures implement subsequent behavioral changes (Egner, 2009; Ridderinkhof et al., 2004). Another line of

¹Department of Physics and Astronomy, Georgia State University, Atlanta, Georgia.

²Neuroscience Institute, Georgia State University, Atlanta, Georgia.

³Center for Behavioral Neuroscience, Center for Nano-Optics, Center for Diagnostics and Therapeutics, GSU-GaTech Center for Advanced Brain Imaging, Georgia State University, Atlanta, Georgia.

evidence suggests that the rAI is a cortical outflow hub of the SN and it coordinates a change in activity across multiple brain networks, including the DMN and CEN (Bonnelle et al., 2012; Menon and Uddin, 2010; Sridharan et al., 2008). In this study, we seek to examine the interactions among the DMN, SN, and CEN, with particular interest in the roles of the rAI and/or DACC in regulating these key networks and their modulations with difficulty of PDM.

We used the traditional left–right motion categorization of moving dots similar to the previous study (Heekeren et al., 2006), conducted an fMRI experiment, and applied the spectral Granger causality (GC) analysis method (Dhamala et al., 2008a, 2008b) to look at the interactions among the DMN, SN, and CEN. We hypothesized that the DMN and CEN would be under causal control from the SN, and if so, a node of the SN would regulate this control. We further hypothesized whether a node that achieved the causal control for easier task would remain the same or change for harder decision-making tasks.

Materials and Methods

Participants

Thirty-two human volunteers (16 males, 16 females; mean age: 27.6 years; standard deviation: 4.7 years) participated in the experiment. All participants reported neurologically healthy and had normal or corrected to normal vision. Written informed consent was collected from each participant before data collection. The experimental protocol was approved from the Institutional Review Board of Center for Advanced Brain Imaging (CABI), Georgia State University and Georgia Institute of Technology. Two participants were excluded from the final analyses because of missing behavior performance records.

Task paradigm

We created random green and red dots. They were presented on a black background and were drawn in a circular aperture. Dots were redrawn after some delay at either a random location or a neighboring spatial location to induce apparent motion to create the resultant motion effect of random dots. The coherence level was determined by the fraction of dots displaced in apparent motion. We presented dots with 12%, 20%, and 50% coherence level (coherence dots were red and green). We also presented 12%, 20%, and 50% coherence dots that had only green color, and they are named color coherence henceforth. The stimuli were presented for 24-sec block, followed by a question mark (“?”), after which time participants responded with a keyboard button press, and then a rest period of 10 sec before starting the next stimulus. We had rest periods of 30 sec at the beginning and at the end of each run. Participants performed two functional runs, each of 810 sec long. The total number of trials was 36 (six trials for each condition). In both sessions, participants categorized random dots as either moving left or right and indicated their decisions by button responses. The presentation software (www.neurobs.com) was used to display the stimuli and to control the task trial sequences.

Data acquisition

Imaging was done on a 3-T Siemens MRI scanner, available at CABI of Georgia State University and Georgia Insti-

tute of Technology. High-resolution T1-weighted anatomical images were acquired first and then followed by two whole-brain functional runs with 405 scans per run with the following parameters: echo-planar imaging, gradient recalled echo sequence; repetition time (TR) = 2000 msec; echo time (TE) = 30 msec; flip angle = 90°; 68 × 68 matrix, voxel dimensions = 3 × 3 × 3 mm³, 37 axial slices each of 3 mm thickness acquired in an interleaved manner with orientation parallel to the anterior–posterior commissural line for the measurement of the T2*-weighted blood oxygenation level-dependent effect. High-resolution anatomical T1-weighted images were acquired for anatomical references using a magnetization-prepared rapid acquisition gradient echo sequence with TR = 2250 msec; TE = 4.18 msec; inversion time = 900 msec; flip angle = 9°; and voxel dimensions = 1 × 1 × 1 mm³.

Data preprocessing

We preprocessed fMRI data using SPM8 (Wellcome Trust Centre for Neuroimaging, London, United Kingdom; www.fil.ion.ucl.ac.uk/spm/software/spm8). Those preprocessing steps included the slice-timing correction, motion correction, coregistration to individual anatomical image, normalization to the Montreal Neurological Institute template, and finally, spatial smoothing of normalized image with a 6-mm isotropic Gaussian kernel.

Selection of regions of interest and extraction of time series

We selected regions of interest (ROIs) using the MarsBaR software package (<http://marsbar.sourceforge.net>) and extracted time courses with the masks on these ROIs. Spherical ROIs were defined as the sets of voxels contained in 6 mm spheres centered on the PCC (7, -43, 33), VMPFC (2, 36, -10), rAI (37, 25, -4), DACC (4, 30, 30), PPC (54, -50, 50), and DLPFC (45, 16, 45). These regions and coordinates were considered based on the previous study by Sridharan and colleagues (2008). Our choice of using the regions only in the right hemisphere was based on the right-lateralized activations reported on the majority of prior neuroimaging studies [e.g., Chen et al. (2013); Sridharan et al. (2008)].

Computation of spectral power and GC

Power spectra were computed using parametric and non-parametric approaches (Chand and Dhamala, 2014; Dhamala et al., 2008a, 2008b). GC spectral analyses are primarily used to examine the strengths, directions, and frequencies of interactions between dynamic processes. The GC spectrum from the second time series X_2 to the first time series X_1 (i.e., $2 \rightarrow 1$) at a frequency (f) is defined as (Dhamala et al., 2008a, 2008b)

$$M_{2 \rightarrow 1}(f) = -\ln \left(1 - \frac{(\sum_{22} - \sum_{12}^2 / \sum_{11}) |H_{12}(f)|^2}{S_{11}(f)} \right), \quad (1)$$

where S is spectral power, H is transfer function, and Σ is noise covariance.

For N nodes, the frequency-specific causal outflow (F) at a node i can be defined as follows:

$$F_i = \frac{1}{N-1} \sum_j^N (M_{i \rightarrow j} - M_{j \rightarrow i}). \quad (2)$$

We used time series extracted from each ROI to compute GC among the nodes of DMN, SN, and CEN. To compute group level GC, time series from all subjects were considered. To obtain the net causal outflow, we first computed GC among all ROIs for each subject, used Equation (2) for each ROI for each subject, and then calculated the mean and standard error of the mean (SEM) over subjects.

The threshold value of GC, for statistical significance, was computed from surrogate data methods by using data permutation calculating GC values and a gamma-function to a distribution of maximum GC values from each permutation (Adhikari et al., 2014; Blair and Karniski, 1993). This threshold was designed to reject a null hypothesis of no interdependence at a significance level of $p < 10^{-3}$.

Results

Behavioral results

The performance (%), which is a ratio of the number of correctly responded trials to the total number of presented trials multiplied by hundred, was calculated for coherence levels of moving dots. Based on *t*-tests, the performance (%) was significantly higher for 50% coherence level (represented as 50% henceforth) compared to the 12% coherence level (represented as 12%). The 20% coherence level did not show statistically significant difference with 50% and 12% coherence levels and hence discarded from subsequent analyses. Only stimuli with 12% color coherence (represented as 12% color coherence) showed statistically significant difference (paired *t*-test) with 12% coherence, and therefore, other color coherence levels (20% and 50% color coherences) were not considered for the subsequent analyses (Fig. 1).

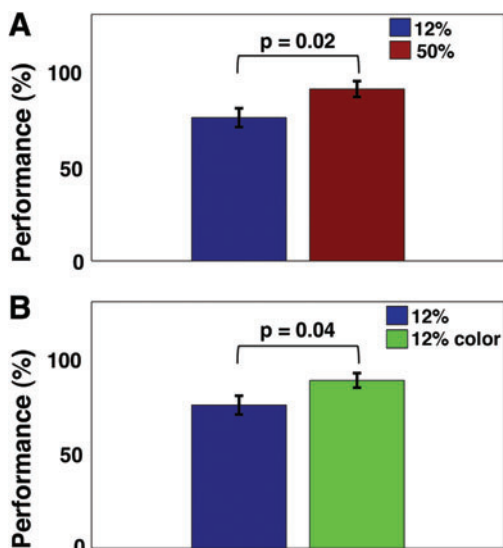


FIG. 1. Behavior responses. (A) Performance (%) was significantly higher for 50% coherence dots compared to 12% coherence dots; (B) performance (%) was significantly higher for 12% color coherence dots compared to 12% coherence dots. $p < 0.05$ indicates statistically significant difference and error bars represent SEM over subjects. SEM, standard error of the mean. Color images available online at www.liebertpub.com/brain

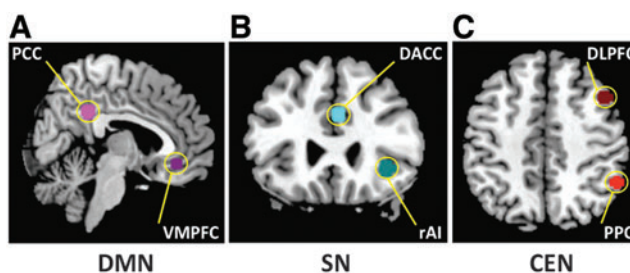


FIG. 2. Selection of the ROIs: (A) PCC and VMPFC of the DMN, (B) rAI and DACC of the SN, and (C) PPC and DLPFC of the CEN. CEN, central-executive network; DACC, dorsal anterior cingulate cortex; DLPFC, dorsolateral prefrontal cortex; DMN, default-mode network; PCC, posterior cingulate cortex; PPC, posterior parietal cortex; rAI, right anterior insula; ROIs, regions of interest; SN, salience network; VMPFC, ventromedial prefrontal cortex. Color images available online at www.liebertpub.com/brain

fMRI results

Individual DMN, SN, and CEN for 50% coherence. Power spectra computed for the nodes of the DMN (the PCC and VMPFC), SN (the rAI and DACC), and CEN (the PPC and DLPFC), respectively, showed peak activities in slow frequency band (0.07–0.19 Hz), often referred as slow-3 band (Bajaj et al., 2013; Zuo et al., 2010), when the participants perceived 50% coherence dots (Fig. 2 and Supplementary Fig. S1; Supplementary Data are available online at www.liebertpub.com/brain). GC spectra were computed to assess the oscillatory network interactions between the nodes of the DMN, SN, and CEN, respectively.

Figure 3 presents GC spectra as a function of frequency, where horizontal lines (Fig. 3A–C) represent a statistically

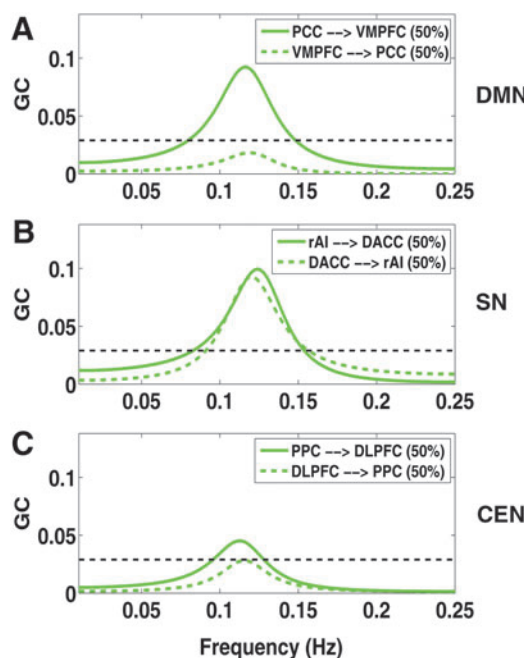


FIG. 3. GC spectra within the (A) DMN, (B) SN, and (C) CEN for 50% coherence dots. GC, Granger causality. Color images available online at www.liebertpub.com/brain

significant threshold value. In the DMN, only the causal flow from the PCC to VMPFC is higher than the threshold value (Fig. 3A). The causal flow is bidirectional between the rAI and DACC in the SN; however, a dominant flow is from the rAI to DACC (Fig. 3B). In the CEN, the causal flow from the PPC to DLPFC is significant but not the other way around. In addition, we also calculated a time-reversed GC (Haufe et al., 2013; Vinck et al., 2015) to cross-validate our GC results. Time-reversed GC calculations demonstrated an altered dominant direction within the DMN, SN, and CEN as expected (Supplementary Fig. S4).

Individual DMN, SN, and CEN for 50% versus 12% coherence. Power spectra computed at the nodes of the DMN (the PCC and VMPFC), SN (the rAI and DACC), and CEN (the PPC and DLPFC), respectively, also showed peak activity in slow-3 band (0.07–0.19 Hz) when the participants perceived 12% coherence dots (Supplementary Fig. S2).

For 12% coherence, dominant causal flow is still from the PCC to VMPFC in the DMN; however, the value is lower than that for 50% coherence (Fig. 4). In the SN, dominant causal flow is still from the rAI to DACC, but with suppressed GC compared to that of 50% coherence. The dominant causal flow is still from the PPC to DLPFC in the CEN.

Individual DMN, SN, and CEN for 12% coherence versus 12% color coherence. Power spectra computed at the nodes of the DMN (the PCC and VMPFC), SN (the rAI and DACC), and CEN (the PPC and DLPFC), respectively, also showed peak activity in slow-3 band (0.07–0.19 Hz) when the participants perceived dots with 12% color coherence (Supplementary Fig. S3).

For 12% color coherence, dominant causal flow is still from the PCC to VMPFC in the DMN; however, its strength

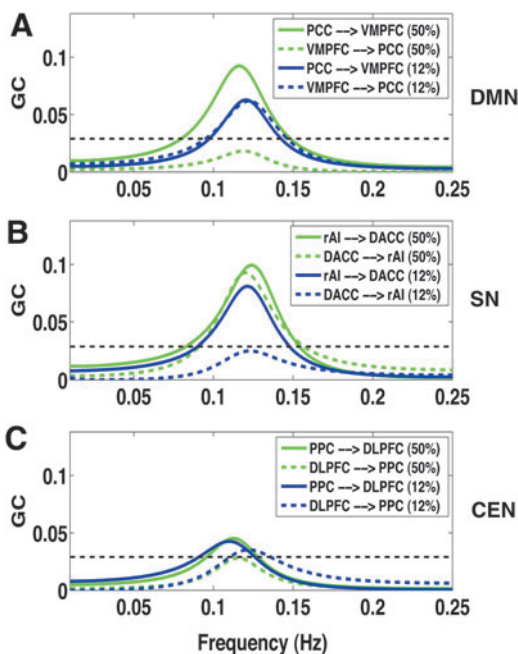


FIG. 4. GC spectra within the (A) DMN, (B) SN, and (C) CEN for 50% and 12% coherence dots. Color images available online at www.liebertpub.com/brain

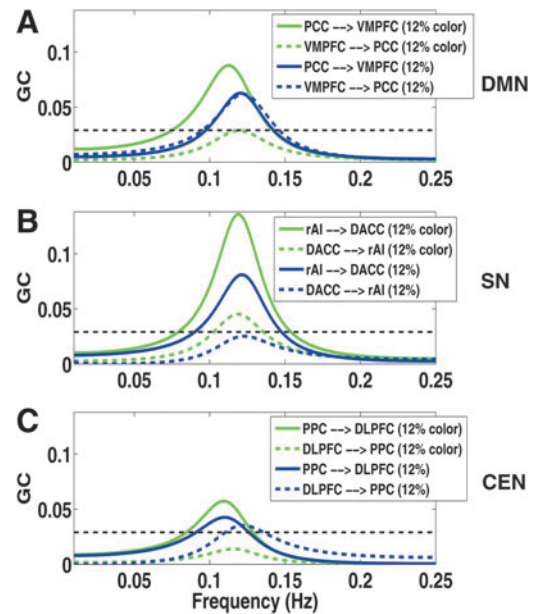


FIG. 5. GC spectra within the (A) DMN, (B) SN, and (C) CEN for 12% coherence and 12% color coherence dots. Color images available online at www.liebertpub.com/brain

is enhanced compared to that for 12% coherence (Fig. 5). In the SN, dominant causal flow is still from the rAI to DACC, but the connectivity strength is enhanced compared to that for 12% coherence. The dominant causal flow is from the PPC to DLPFC in the CEN in 12% color coherence.

Causal interaction among the DMN, SN, and CEN. In 50% coherence dots, we computed net causal outflow (out-in degree) at the key nodes of the SN, CEN, and DMN. The comparison of the net causal outflows revealed that the rAI had a significantly higher causal control over the DACC and the nodes of the DMN and CEN (Fig. 6A).

We further calculated net causal outflows for 12% coherence dots, which is a harder task compared to 50% coherence as reflected from behavioral measures (Fig. 1A). In 12% coherence dots (Fig. 6B), comparison of the net causal outflows among the key nodes of the SN, CEN, and DMN uncovered that, in addition to the rAI, the DACC had a significantly higher causal control over the CEN and DMN regions (Supplementary Fig. S5 for 20% coherence dots). The net causal outflow comparison between the rAI and DACC is not significantly different. We further calculated net causal outflow for 12% color coherence, which is an easier task compared to 12% coherence as reflected from behavioral measures (Fig. 1B). For 12% color coherence dots, comparison of the net causal outflows among the key nodes of the SN, CEN, and DMN revealed that the rAI had a significantly higher net causal outflow than the CEN and DMN regions (Fig. 6C). The net causal outflows of the rAI and DACC are not significantly different, but showed an enhanced causal outflow of the rAI and a suppressed causal outflow of the DACC compared to the 12% coherence (Fig. 6B, C).

Discussion

We demonstrated that an individual DMN, SN, and CEN had dominantly feed-forward network activity mediated by

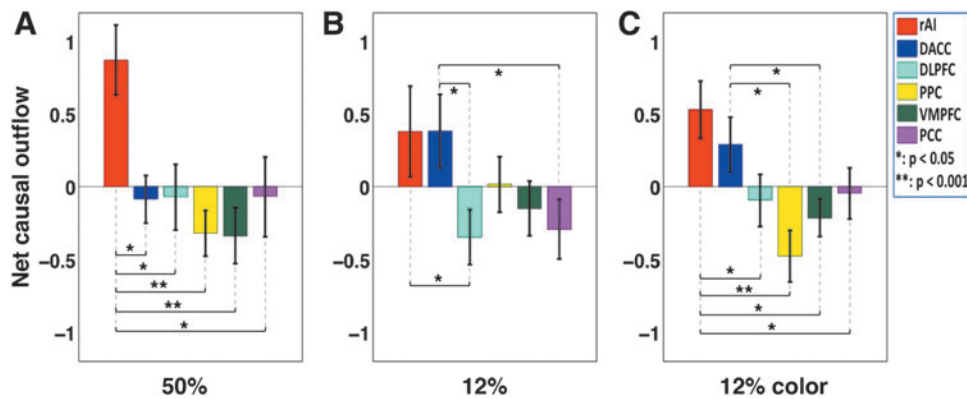


FIG. 6. Net causal outflow of the key nodes of the SN, CEN, and DMN. (A) The rAI had a significantly higher net causal outflow compared to the DACC, and the CEN and DMN nodes for 50% coherence dots, (B) both rAI and DACC, especially the DACC, had a significantly higher net causal outflow compared to the CEN and DMN nodes for coherence and 12% coherence dots, and (C) the rAI and DACC had a significantly higher net causal outflow compared to the CEN and DMN nodes for 12% color coherence dots. $p < 0.05$ indicates statistically significant difference and error bars represent SEM over subjects. *represents $p < 0.05$; **represents $p < 0.001$. Color images available online at www.liebertpub.com/brain

slow-frequency band (0.07–0.19 Hz) often referred as slow-3 band (Bajaj et al., 2013; Zuo et al., 2010). We found two important results that showed organization of sensory information among the DMN, SN, and CEN. First, the rAI of the SN played causal control over the DMN and CEN for easier decision, which is consistent with previous investigation for different sensory information-driven, goal-directed tasks (Sridharan et al., 2008). Second, the rAI played a relatively lower causal control and the rAI and DACC exerted a causal control over the DMN and CEN (Fig. 6B). Moreover, when color dots were present (12% color coherence), task became behaviorally easier and an increased role of rAI (compared to 12% coherence) was observed (Fig. 6C).

Recent studies have consistently demonstrated that the rAI of the SN drives the DMN and CEN for different tasks (Goulden et al., 2014; Sridharan et al., 2008). Our results for easier decision-making tasks also replicated those existing studies. In addition, our result for harder decision-making tasks demonstrated further that both the rAI and DACC of the SN causally control the DMN and CEN. Anatomically, the AI and anterior cingulate cortex (ACC) are a part of a network (Critchley et al., 2004) and also share a unique feature at the neuronal level. The von Economo neurons (VENs)—a special type of neuron exclusively localized to the AI and ACC—relay information processed within the AI and ACC to other parts of the brain (Allman et al., 2005; Watson et al., 2006). The control signals generated by the rAI (for easier decisions) and by both the DACC and rAI (for harder decisions) might be supported by the neuronal basis of control signals of the VENs. Previous studies of attention and cognitive control have reported coactivation of the rAI and DACC (Crottaz-Herbette and Menon, 2006; Dosenbach et al., 2006; Ham et al., 2013), but their differential functional roles are still in debate. The rAI is functionally connected to the networks responsible for adaptive behavior, including the SN (Seeley et al., 2007), as well as other parts of the frontoparietal control network (Vincent et al., 2008). Diffusion tensor imaging demonstrated that this cortical area has direct white matter connections to other key regions, including the DACC (van den Heuvel et al., 2009), the inferior parietal lobe (Uddin et al., 2010), and the

temporoparietal junction (Kucyi et al., 2012), making the insula (rAI) well placed to perform its putative role of evaluating (Uddin et al., 2010), reorienting attention (Ullsperger et al., 2010), and switching between cognitive resources in response to salient events (Uddin and Menon, 2009), similar to the line that we found for easier decisions. In contrast, the activity in the DACC is known to signal the need for enhanced cognitive control (Ridderinkhof et al., 2004) and to implement behavioral changes (Egner, 2009; Ridderinkhof et al., 2004). Our results for harder decisions might implicate the role of the DACC for an enhanced cognitive control (Egner, 2009; Ridderinkhof et al., 2004) especially when sensory information is limited (harder decisions). Our findings for both easier and harder decisions therefore provide strong evidence for the neural basis of rAI–DACC network to initiate control signals in sensory information-driven, goal-directed tasks (Allman et al., 2005; Watson et al., 2006).

In conclusion, we evaluated the patterns of interactions among DMN, SN, and CEN in perceptual decisions of moving dots. We found that the slow-3 oscillation (0.07–0.19 Hz) mediated interaction within and between these networks, the rAI of the SN played causal control over the DMN and CEN for easier decisions, and finally, both the rAI and DACC of the SN sent causal control in harder decisions. These findings advance our current understanding of how sensory signal organizes among the DMN, SN, and CEN for sensory-information, goal-directed tasks, including easier and harder perceptual decisions.

Acknowledgments

The authors thank Crystal Smith for writing computer programs to control and present the stimuli, Drs. Bidhan Lamichhane and Bhim Adhikari for the data collection, and Timothy Jordan for proofreading the manuscript. A National Science Foundation CAREER award (BCS 0955037) was given to the author MD financially supporting this work.

Author Disclosure Statement

No competing financial interests exist.

References

- Adhikari BM, Sathian K, Epstein CM, Lamichhane B, Dhamala M. 2014. Oscillatory activity in neocortical networks during tactile discrimination near the limit of spatial acuity. *Neuroimage* 91:300–310.
- Allman JM, Watson KK, Tetreault NA, Hakeem AY. 2005. Intuition and autism: a possible role for Von Economo neurons. *Trends Cogn Sci* 9:367–373.
- Bajaj S, Adhikari BM, Dhamala M. 2013. Higher frequency network activity flow predicts lower frequency node activity in intrinsic low-frequency BOLD fluctuations. *PLoS One* 8:e64466.
- Becerra L, Pendse G, Chang PC, Bishop J, Borsook D. 2011. Robust reproducible resting state networks in the awake rodent brain. *PLoS One* 6:e25701.
- Blair RC, Karniski W. 1993. An alternative method for significance testing of waveform difference potentials. *Psychophysiology* 30:518–524.
- Bonnelle V, Ham TE, Leech R, Kinnunen KM, Mehta MA, Greenwood RJ, Sharp DJ. 2012. Salience network integrity predicts default mode network function after traumatic brain injury. *Proc Natl Acad Sci U S A* 109:4690–4695.
- Chand GB, Dhamala M. 2014. Spectral factorization-based current source density analysis of ongoing neural oscillations. *J Neurosci Methods* 224:58–65.
- Chen AC, Oathes DJ, Chang C, Bradley T, Zhou ZW, Williams LM, Glover GH, Deisseroth K, Etkin A. 2013. Causal interactions between fronto-parietal central executive and default-mode networks in humans. *Proc Natl Acad Sci U S A* 110:19944–19949.
- Critchley HD, Wiens S, Rotshtein P, Ohman A, Dolan RJ. 2004. Neural systems supporting interoceptive awareness. *Nat Neurosci* 7:189–195.
- Crottaz-Herbette S, Menon V. 2006. Where and when the anterior cingulate cortex modulates attentional response: combined fMRI and ERP evidence. *J Cogn Neurosci* 18:766–780.
- Deco G, Jirsa VK, McIntosh AR. 2011. Emerging concepts for the dynamical organization of resting-state activity in the brain. *Nat Rev Neurosci* 12:43–56.
- Dhamala M, Rangarajan G, Ding M. 2008a. Analyzing information flow in brain networks with nonparametric Granger causality. *Neuroimage* 41:354–362.
- Dhamala M, Rangarajan G, Ding M. 2008b. Estimating Granger causality from Fourier and wavelet transforms of time series data. *Phys Rev Lett* 100:018701.
- Dosenbach NU, Visscher KM, Palmer ED, Miezin FM, Wenger KK, Kang HC, Burgund ED, Grimes AL, Schlaggar BL, Petersen SE. 2006. A core system for the implementation of task sets. *Neuron* 50:799–812.
- Egner T. 2009. Prefrontal cortex and cognitive control: motivating functional hierarchies. *Nat Neurosci* 12:821–822.
- Fox MD, Snyder AZ, Vincent JL, Corbetta M, Van Essen DC, Raichle ME. 2005. The human brain is intrinsically organized into dynamic, anticorrelated functional networks. *Proc Natl Acad Sci U S A* 102:9673–9678.
- Fransson P. 2005. Spontaneous low-frequency BOLD signal fluctuations: an fMRI investigation of the resting-state default mode of brain function hypothesis. *Hum Brain Mapp* 26:15–29.
- Goulden N, Khusnulina A, Davis NJ, Bracewell RM, Bokde AL, McNulty JP, Mullins PG. 2014. The salience network is responsible for switching between the default mode network and the central executive network: replication from DCM. *NeuroImage* 99:180–190.
- Ham T, Leff A, de Boissezon X, Joffe A, Sharp DJ. 2013. Cognitive control and the salience network: an investigation of error processing and effective connectivity. *J Neurosci* 33:7091–7098.
- Heekeren HR, Marrett S, Ruff DA, Bandettini PA, Ungerleider LG. 2006. Involvement of human left dorsolateral prefrontal cortex in perceptual decision making is independent of response modality. *Proc Natl Acad Sci U S A* 103:10023–10028.
- Haufe, et al. 2013. A critical assessment of connectivity measures for EEG data: a simulation study. *NeuroImage* 64:120–133.
- Kucyi A, Moayed M, Weissman-Fogel I, Hodaie M, Davis KD. 2012. Hemispheric asymmetry in white matter connectivity of the temporoparietal junction with the insula and prefrontal cortex. *PLoS One* 7:e35589.
- Menon V, Uddin LQ. 2010. Saliency, switching, attention and control: a network model of insula function. *Brain Struct Funct* 214:655–667.
- Power JD, Cohen AL, Nelson SM, Wig GS, Barnes KA, Church JA, Vogel AC, Laumann TO, Miezin FM, Schlaggar BL, Petersen SE. 2011. Functional network organization of the human brain. *Neuron* 72:665–678.
- Ridderinkhof KR, Ullsperger M, Crone EA, Nieuwenhuis S. 2004. The role of the medial frontal cortex in cognitive control. *Science* 306:443–447.
- Seeley WW, Menon V, Schatzberg AF, Keller J, Glover GH, Kenna H, Reiss AL, Greicius MD. 2007. Dissociable intrinsic connectivity networks for salience processing and executive control. *J Neurosci* 27:2349–2356.
- Sridharan D, Levitin DJ, Menon V. 2008. A critical role for the right fronto-insular cortex in switching between central-executive and default-mode networks. *Proc Natl Acad Sci U S A* 105:12569–12574.
- Uddin LQ. 2015. Saliency processing and insular cortical function and dysfunction. *Nat Rev Neurosci* 16:55–61.
- Uddin LQ, Menon V. 2009. The anterior insula in autism: under-connected and under-examined. *Neurosci Biobehav Rev* 33:1198–1203.
- Uddin LQ, Supekar K, Amin H, Rykhlevskaia E, Nguyen DA, Greicius MD, Menon V. 2010. Dissociable connectivity within human angular gyrus and intraparietal sulcus: evidence from functional and structural connectivity. *Cereb Cortex* 20:2636–2646.
- Ullsperger M, Harsay HA, Wessel JR, Ridderinkhof KR. 2010. Conscious perception of errors and its relation to the anterior insula. *Brain Struct Funct* 214:629–643.
- van den Heuvel MP, Mandl RC, Kahn RS, Hulshoff Pol HE. 2009. Functionally linked resting-state networks reflect the underlying structural connectivity architecture of the human brain. *Hum Brain Mapp* 30:3127–3141.
- Vincent JL, Kahn I, Snyder AZ, Raichle ME, Buckner RL. 2008. Evidence for a frontoparietal control system revealed by intrinsic functional connectivity. *J Neurophysiol* 100:3328–3342.
- Vinck, et al. 2015. How to detect the Granger-causal flow direction in the presence of additive noise? *NeuroImage* 108:301–318.
- Watson KK, Jones TK, Allman JM. 2006. Dendritic architecture of the von Economo neurons. *Neuroscience* 141:1107–1112.
- Zuo XN, Di Martino A, Kelly C, Shehzad ZE, Gee DG, Klein DF, Castellanos FX, Biswal BB, Milham MP. 2010. The oscillating brain: complex and reliable. *Neuroimage* 49:1432–1445.

Address correspondence to:

Ganesh B. Chand
 Department of Physics and Astronomy
 Georgia State University
 1 Park Place NE, Suite 439B
 Atlanta, GA 30303

E-mail: gchand1@student.gsu.edu